ELECTRON PERFORMANCE WITH J/ψ WITH THE ATLAS DETECTOR*

Timothée Theveneaux-Pelzer

on behalf of the ATLAS Collaboration

Laboratoire de Physique Nucléaire et de Hautes Energies
UPMC and Université Paris-Diderot and CNRS/IN2P3, Paris, France

(Received April 29, 2011)

This paper describes the performance of low energy electron reconstruction and identification at ATLAS with proton–proton collisions at a centre of mass energy of 7 TeV produced by the Large Hadron Collider. This study was performed with a sample collected from April to June 2010, corresponding to an integrated luminosity of 78 nb^{-1}. We present the reconstruction of prompt J/ψ mesons decaying into e^+e^- pairs. These electrons can be used to study the detector performance at low energy, as a complement of higher energy electrons coming from W and Z decays. A sample of ~ 220 J/ψ events can be selected. Their mass values reconstructed with different inputs agree with the values expected from the initial calibration of the ATLAS detector. The kinematics and shower shape distributions (used for identification purpose) have been extracted from the J/ψ data sample and show a good agreement with the simulation.

DOI:10.5506/APhysPolB.42.1645
PACS numbers: 13.20.Gd, 14.60.Cd

1. Introduction

The ATLAS detector has been running in 2010, collecting data from proton–proton collisions with a centre of mass energy of 7 TeV produced by the LHC, corresponding to an integrated luminosity of 45 pb^{-1} [1], with a data-recording efficiency of $\sim 93.6\%$. Figure 1 (a) shows the di-electron invariant mass distribution obtained with the first 10 pb^{-1} of ATLAS data. The J/ψ is the most abundant source of isolated electrons in ATLAS. Along

* Presented at the Cracow Epiphany Conference on the First Year of the LHC, Cracow, Poland, January 10–12, 2011.

[1] The systematic uncertainty on the luminosity was 11% at the time of this paper, mostly due to measurement of LHC beam currents [1].

with the Z boson, it is one of the few "standard candles" that will be used to calibrate the detector and measure the electron identification efficiency. We present the observation of $J/\psi \to ee$ decays with the first 78 nb^{-1}, which has proved to be challenging due to the low transverse momentum (p_{T}) spectrum of the J/ψ (Fig. 1 (b)) and the large hadronic background.

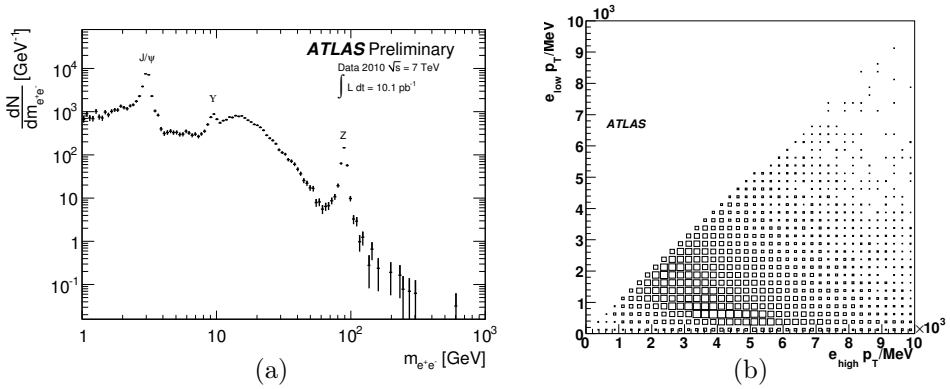

Fig. 1. (a) Distribution of opposite sign di-electron invariant mass for the first 10.1 pb^{-1} of 2010 data collected with a di-electron trigger with a transverse energy (E_{T}) threshold of 5 GeV [2]. (b) Distribution of the generator-level transverse momentum of the less energetic electron *versus* the transverse momentum of the most energetic electron in 14 TeV simulation of direct J/ψ decays [3].

A Monte Carlo sample of prompt $J/\psi \to ee$ events was generated with Pythia 6.4 [4], using the colour singlet and octet production mechanisms. Contributions of radiative decays of prompt χ_{c1} are expected to have similar kinematics properties, and contributions of J/ψ non-prompt production from b-quark are not important for the distributions studied at this stage. The generated events are passing through a detailed simulation of the ATLAS detector based on GEANT4 [5] and are reconstructed with the same software as used for the data.

A brief overview of the ATLAS detector is given in Sec. 2. The electron trigger, reconstruction and identification procedures are detailed in Sec. 3, emphasizing the variations with respect to the standard reconstruction and identification necessary to maximise the statistics on low p_{T} electrons with first data. In Sec. 4 the performance studies on electrons from J/ψ are presented.

2. The ATLAS detector

The ATLAS detector is made of several sub-detectors with a cylindrical geometry to cover the full acceptance. A detailed description can be found in [6]. The two main sub-systems used in the reconstruction and identi-

fication of electrons are the inner tracker and the electromagnetic (EM) calorimeter. Closest to the beam-pipe, the inner detector is immersed in a 2 T solenoidal magnetic field and provides tracking information in the precision measurement pseudo-rapidity range of the EM calorimeter. It is made of a pixel silicon detector — allowing precise measurement of vertex position — surrounded by a silicon micro-strips detector (Semi Conductor Tracker, SCT) and by a Transition Radiation Tracker (TRT). Both pixel and SCT cover the same pseudo-rapidity range $|\eta| < 2.5$ whereas the TRT extends only up to $|\eta| = 2.0$. A charged particle creates a track with typically 3 pixel hits, 8 SCT hits (*i.e.* 4 space points), and about 36 TRT hits. The TRT provides discriminating power between electrons and pions by the detection of transition radiation in the xenon-based gas mixture of the straw tubes.

The lead/liquid argon (LAr) sampling EM calorimeter is divided into a barrel part ($|\eta| < 1.475$) and two end-caps ($1.375 < |\eta| < 3.2$). Over the region devoted to precision physics ($|\eta| < 2.5$) the EM calorimeter is segmented in three layers in depth. For high energy objects, most of the EM shower energy is collected in the second layer which has a granularity of 0.025×0.025 in $\eta \times \phi$ space. The first layer has a finer segmentation in η — allowing an excellent γ/π^0 discrimination — but a coarser segmentation in ϕ. This granularity is 0.0031×0.1 in the barrel calorimeter. The third layer has a granularity of 0.05×0.025. To take into account the energy losses of the particles upstream the calorimeter, a thin LAr presampler with coarse granularity is used in the $|\eta| < 1.8$ region.

3. Electron trigger, reconstruction and identification

3.1. Electron trigger

Events are selected with a three level trigger, reducing the data acquisition rate to ~ 300 Hz. The level 1 (L1) trigger selects regions of interest (RoI) in the EM calorimeter with a transverse energy above a threshold. The level 2 (L2) trigger performs a fast reconstruction of the events and refines the selection of the RoI using the inner tracker and the full calorimeter granularity. The event filter (EF) performs a full reconstruction of the events and applies standard identification criteria to the objects selected by L2. L1 is a hardware trigger, whereas L2 and EF are software triggers, and are called together High Level Triggers (HLT).

In 2010, the luminosity delivered by the LHC increased almost exponentially, thanks to machine improvements. The data taking started with an instantaneous luminosity of $\sim 10^{28}\mathrm{cm}^{-2}\mathrm{s}^{-1}$ and reached the record of $2.1 \times 10^{32}\mathrm{cm}^{-2}\mathrm{s}^{-1}$ for proton–proton collisions in October. To keep the data recording rate within the processing capabilities, a random fraction of the data selected by the trigger system has to be rejected. The rejection fac-

tor (prescale rate) of each trigger increases with instantaneous luminosity. Figure 2 shows the data-taking rates for L1 triggers before prescale, for a luminosity up to $7 \times 10^{29}\text{cm}^{-2}\text{s}^{-1}$. In this analysis, for the first data-taking period a trigger requiring a single hit in one of trigger scintillators mounted on each side of the experiment was used. Then, with the increase of the luminosity we selected events with a L1 trigger requiring an EM cluster of size $\Delta\eta \times \Delta\phi = 0.1 \times 0.1$ within the $|\eta| < 2.5$ region with transverse energy of at least 3 GeV. For the last data-taking periods used in this analysis, similar calorimeter triggers with an E_{T} threshold of 3 GeV were used but performed by the HLT with additional identification criteria.

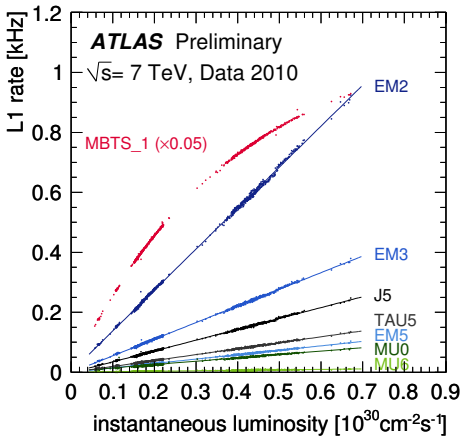

Fig. 2. L1 rates before prescale as a function of luminosity for EM triggers ($E_{\text{T}} > 2$, 3 and 5 GeV), muon triggers ($p_{\text{T}} > 0$ and 6 GeV), a tau trigger ($E_{\text{T}} > 5$ GeV), a jet trigger ($E_{\text{T}} > 5$ GeV) and a trigger requiring a single hit in a minimum bias trigger scintillator (MBTS_1). MBTS_1 saturation is due to pile-up, and its rate is divided by 20 in the figure.

3.2. Electron reconstruction

The electron reconstruction begins with the creation of seed energy clusters in the EM calorimeter with significant energy. In the standard "sliding window" algorithm, optimised for high E_{T} electrons like the ones from Z, seed clusters are a fixed-size rectangular window — $\Delta\eta \times \Delta\phi = 3 \times 5$ in units of the EM calorimeter middle layer cell size of 0.025×0.025 — with $E_{\text{T}} > 2.5$ GeV. Electrons are reconstructed from these clusters if there is a suitable match with a track of $p_{\text{T}} > 0.5$ GeV. The associated track is chosen to be the one with the closest distance between the extrapolation at the calorimeter and the cluster barycentre in the EM calorimeter. However, for

the $J/\psi \rightarrow ee$ study with early data a nearest-neighbour clustering algorithm was used since it improves the reconstruction efficiency at low energy due to its lower threshold ($E_{\mathrm{T}} > 300$ MeV). These topological clusters are constructed by aggregating a seed cell with $E > 4\sigma$, with surrounding cells with $E > 2\sigma$, where σ is the expected electronic noise.

From these seed clusters, rectangular clusters are built. The optimal size for electron candidates is 3×7 cells in $\eta \times \phi$ in the barrel of the EM calorimeter and 5×5 in the end-caps. A layer weighted calibration scheme is used to compute the cluster energy and correct for the energy losses and optimize the resolution in this low energy regime.

3.3. Electron identification

The standard electron identification in ATLAS relies on rectangular cuts on a set of variables delivering good separation between isolated electrons and jets. Three reference sets of cuts have been defined which have progressively stronger jet rejection factor and decreasing efficiency. For loose selection cuts on hadronic leakage and lateral shower shapes in the second sampling of the EM calorimeter are applied. For medium selection cuts on lateral shower shapes in the first sampling, on track quality variables and on track matching variables are applied in addition to loose cuts. For tight selection, cuts on TRT variables and tighter cuts on track quality and track matching are applied in addition to medium cuts.

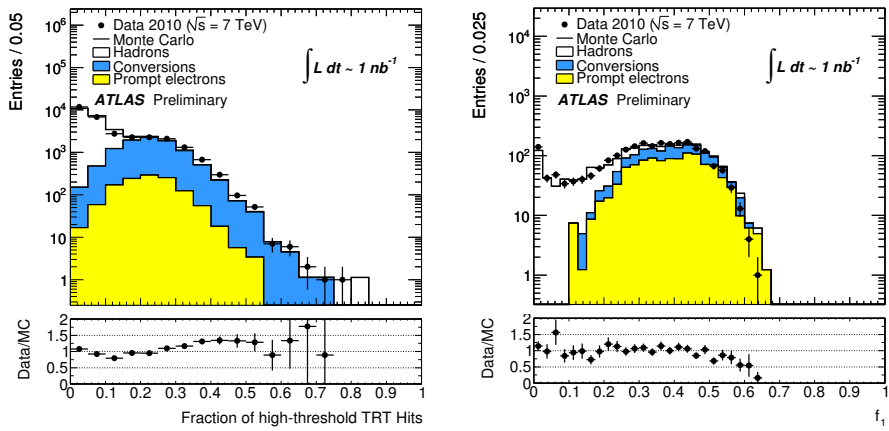

(a) (b)

Fig. 3. Comparison of the distributions in data and in simulation of two discriminating variables used in the standard identification scheme, for an inclusive electron analysis based on 1 nb^{-1} [7]. (a) $\mathrm{TRT_{frac}}$: fraction of hits passing high level threshold in TRT, after loose selection. (b) f1: fraction of energy reconstructed in the first layer of the EM calorimeter, after tight selection.

The baseline identification was optimised for high p_{T} electrons. Therefore, for this analysis on the very first data, a subset of these variables were used and the cuts re-optimised to maximise the signal over background ratio. In particular, low energy electrons strongly rely on the number of hits in the silicon trackers, on the fraction of hits in the TRT passing high transition radiation threshold cut ($\mathrm{TRT}_{\mathrm{frac}}$, Fig. 3 (a)), on the fraction of energy deposited in the first layer on the EM calorimeter (f1, Fig. 3 (b)) and on the lateral shower containment in the η direction.

4. Electron performance with $J/\psi \to ee$ on first data

4.1. Selection

Events containing at least two electrons were selected. The electrons are required to be within the TRT fiducial pseudo-rapidity region $|\eta| < 2.0$, and the transition region $1.37 < |\eta| < 1.52$ between barrel and end-cap calorimeters is excluded. The transverse momentum of the electrons must be greater than 2 GeV. We require the electrons to pass track quality cuts: at least 1 pixel hit, at least 1 hit in the innermost pixel layer in order to reduce the background from converted photons, and at least 7 hits in the silicon detectors. The closest distance to the vertex of the electron track (d_0) is required to be less than $5\sigma_{d_0}$, where σ_{d_0} is the associated uncertainty on d_0. The fraction of hits passing high level threshold in TRT ($\mathrm{TRT}_{\mathrm{frac}}$) must be at least 0.12. To remove hadrons which give larger EM showers, the ratio of the energy of the cells in a 3×7 over 7×7 in the middle layer of the EM calorimeter (R_η) must be smaller than 0.85(0.9) in the barrel (end-caps) region. The fraction of energy deposited in the first layer (f1) must be at least 0.15, and the two largest energy deposits in this layer must have a difference greater than 7% of their sum ($E_{\mathrm{ratio}} > 0.07$).

We select electron pairs of opposite charges with tighter requirements on one electron: the transverse momentum of the track must be greater than 4 GeV, the transverse energy of the cluster greater than 2.5 GeV, and $\mathrm{TRT}_{\mathrm{frac}}$ greater than 0.18.

4.2. J/ψ mass distribution

Two approaches are used for calculating the mass of the electron pairs. The first one consists in using the energy of the electron cluster combined with η and ϕ measured from the track. The stochastic term of the energy resolution function of the EM calorimeter is expected to be $10\%\sqrt{E/\mathrm{GeV}}$, giving at low p_{T} a resolution worse than the track momentum resolution ($\sim 2\%$). Therefore the mass can be computed from track parameters only. The default tracking algorithm performs a global χ^2 fit, using a Kalman

filter [8] which does not take into account the energy losses of the electron due to Bremsstrahlung effect, giving underestimated electron momenta. This can be corrected by using a Gaussian Sum Filter (GSF) algorithm [9].

Figure 4 shows the distributions of the invariant mass of electron pairs. The difference with the nominal J/ψ mass (3.096 ± 0.011 GeV [13]) observed when calculating the invariant mass of electron pairs from calorimeter cluster energy and track direction (Fig. 4 (a)) is explained by the expected 3% uncertainty on the initial energy scale and by the non-nominal calibration at these low energies (*cf.* Table I). The signal yield is estimated in the whole 1.5 to 4 GeV fitting range, whereas the background yield is estimated between $M - 3\sigma_M$ and $M + 2\sigma_M$, where M is the fitted J/ψ mass and σ_M the width of the distribution. When calculating the invariant mass from

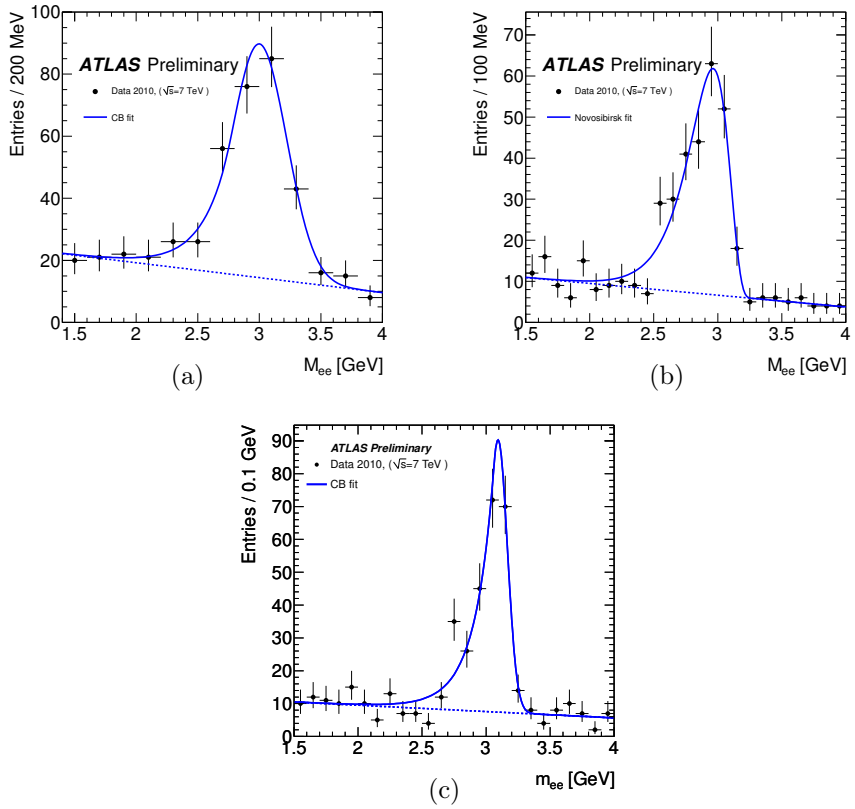

Fig. 4. Invariant mass of the electron pairs calculated from calorimeter energy and track direction (a), from track parameters only (b) and from track parameters with refit to take into account Bremsstrahlung effect (c) [10]. The signal is fitted with Crystal Ball function [11] for (a) and (c), and with Novosibirsk function [12] for (b). The background is fitted with a linear parametrization.

track parameters only (Fig. 4 (b)), the width is smaller, giving a better signal over background ratio — ~ 4.1 instead of ~ 2.4 — which is due to the smaller area to estimate the signal and background yields. The J/ψ mass is still lower than the nominal value. Taking into account the Bremsstrahlung effect in the track fitting (Fig. 4 (c)) gives a better signal over background ratio (~ 7.9) thanks to the much smaller σ_M. In the latter case the J/ψ mass is much closer to the nominal value.

TABLE I

Parameters of the fits of the three invariant mass distributions shown in Fig. 4: J/ψ mass (M), total width (σ_M), number of signal events ($N_{\rm sig}$) and number of background events ($N_{\rm bkg}$). $N_{\rm sig}$ and $N_{\rm bkg}$ are calculated from $M-3\sigma_M$ to $M+2\sigma_M$.

Mass measurement method	M [GeV]	σ_M [GeV]	$N_{\rm sig}$	$N_{\rm bkg}$
E(cluster), η(track), ϕ(track)	3.00 ± 0.03	0.22 ± 0.03	229 ± 24	96 ± 22
Tracks parameters only	2.96 ± 0.01	0.16 ± 0.01	234 ± 20	57 ± 18
Tracks parameters with GSF refit	3.09 ± 0.01	0.07 ± 0.01	222 ± 11	28 ± 2

4.3. J/ψ kinematics distributions

The J/ψ candidates kinematics distributions are obtained by selecting the electron pairs with a track invariant mass between 2.5 and 3.2 GeV (Fig. 5). The distributions from data are compared to direct $J/\psi \to ee$ simulation. The agreement is good, however some slight differences are observed at low $p_{\rm T}$ which can be partially explained by the contribution of non direct J/ψ production.

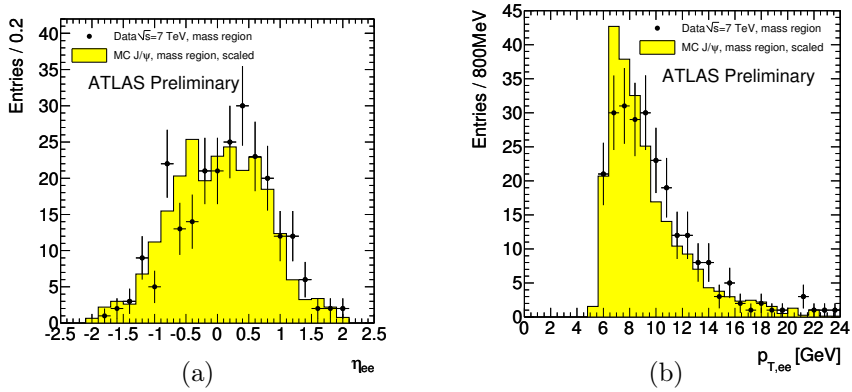

Fig. 5. Kinematic distributions of J/ψ candidates: pseudo-rapidity (a) and transverse momentum (b). The data are compared to direct $J/\psi \to ee$ simulation, scaled to data [10].

4.4. Extraction of shower shapes

The J/ψ signal can be used to extract the electron shower shapes. To do so, the cuts on the discriminating variables on the electron with loosest cuts ($p_{\mathrm{T}} > 2$ GeV) are removed, except $f_1 > 0.15$. The electron pairs are selected if their invariant mass is between 2.7 and 3.2 GeV.

Figure 6 shows a comparison between data and simulation of two variables, f_1 and W_{tot} — the shower width in the η direction for the first layer of the EM calorimeter. The agreement between data and simulation is good. Even though, small systematic effects emerge, in particular the shower width (W_{tot}) is larger in data. These effects cannot be explained by the remaining $\sim 15\%$ of background, and seems to indicate a not enough accurate description of the shower profile in the simulation. These explanations are still under study.

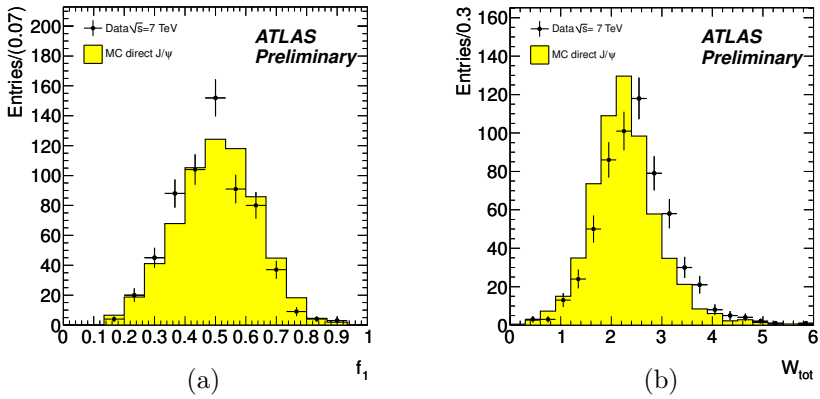

Fig. 6. Distributions of f_1 and W_{tot} for data, compared to direct $J/\psi \to ee$ simulation, scaled to data [10]. (a) f_1: fraction of energy in the first layer relative to all three layers of the EM calorimeter. (b) W_{tot}: Shower width in the η direction for the first layer of the EM calorimeter (in units of strips).

5. Conclusion

The first year of data taking with $\sqrt{s} = 7$ TeV has been mainly devoted to test our understanding of the performance of the ATLAS detector. The first $J/\psi \to ee$ signal was extracted with a dedicated reconstruction and identification. With 78 nb^{-1}, about 220 J/ψ were observed with mass values in agreement with the expected one from the J/ψ, taking into account the initial calibration and energy scale. Low-p_{T} electron distributions were extracted from the J/ψ data sample. Kinematics distributions agree well with the simulation while small discrepancies have been observed on some shower variables. Explanation for these differences is still under study with the full 2010 data sample and using also the high p_{T} electron sample.

REFERENCES

[1] [ATLAS Collaboration] G. Aad *et al.*, *Eur. Phys. J.* **C71**, 1630 (2011) [arXiv:1101.2185v1 [hep-ex]].

[2] [ATLAS Collaboration] G. Aad *et al.*, https://atlas.web.cern.ch/Atlas/GROUPS/PHYSICS/EGAMMA/PublicPlots/20101110/eeSpectrum/ATL-COM-PHYS-2010-882/index.html

[3] [ATLAS Collaboration] G. Aad *et al.*, arXiv:0901.0512v4 [hep-ex].

[4] T. Sjöstrand, S. Mrenna, P. Skands, *J. High Energy Phys.* **0605**, 026 (2006).

[5] S. Agostinelli *et al.*, *Nucl. Instrum. Methods* **506**, 250 (2003).

[6] [ATLAS Collaboration] G. Aad *et al.*, *JINST* **3**, S08003 (2008).

[7] [ATLAS Collaboration] G. Aad *et al.*, https://atlas.web.cern.ch/Atlas/GROUPS/PHYSICS/EGAMMA/PublicPlots/20100602/ATL-COM-PHYS-2010-302/index.html

[8] T.G. Cornelissen, Track Fitting in the ATLAS Experiment, PhD thesis, Univ. Amsterdam, CERN-THESIS-2006-072, 2006.

[9] V. Kartvelishvili, *Nucl. Phys. B (Proc. Suppl.)* **172**, 208 (2007).

[10] [ATLAS Collaboration] G. Aad *et al.*, https://atlas.web.cern.ch/Atlas/GROUPS/PHYSICS/EGAMMA/PublicPlots/20100721/ATL-COM-PHYS-2010-518/index.html

[11] M.J. Oreglia, A Study of the Reactions $\psi' \to \gamma\psi$, SLAC-R-236, Appendix D, 1980.

[12] B. Aubert *et al.*, *Phys. Rev.* **D70**, 112006 (2004).

[13] [Particle Data Group] K. Nakamura *et al.*, *J. Phys. G* **37**, 075021 (2010).